ChemPubSoc Europe

DOI: 10.1002/chem.201402415

CHEMISTRY
A European Journal
Full Paper

Lanthanide Complexes

Comparative Analysis of Conjugated Alkynyl Chromophore–Triazacyclononane Ligands for Sensitized Emission of Europium and Terbium

Marine Soulié,[a] Frédéric Latzko,[a] Emmanuel Bourrier,[a] Virginie Placide,[b] Stephen J. Butler,[c] Robert Pal,[c] James W. Walton,[c] Patrice L. Baldeck,[b, e] Boris Le Guennic,[d] Chantal Andraud,[b] Jurriaan M. Zwier,[a] Laurent Lamarque,*[a] David Parker,*[c] and Olivier Maury*[b]

Abstract: A series of europium and terbium complexes based on a functionalized triazacyclononane carboxylate or phosphinate macrocyclic ligand is described. The influence of the anionic group, that is, carboxylate, methylphosphinate, or phenylphosphinate, on the photophysical properties was studied and rationalized on the basis of DFT calculated structures. The nature, number, and position of electron-donating or electron-withdrawing aryl substituents were varied systematically within the same phenylethynyl scaffold in order to optimize the brightness of the corresponding europium complexes and investigate their two-photon absorption properties. Finally, the europium complexes were examined in cell-imaging applications, and selected terbium complexes were studied as potential oxygen sensors.

Introduction

In the last two decades, various aspects of f-element spectroscopy have been extensively studied,[1] and lanthanide coordination complexes in particular have found important applications in the biological sciences.[2] In this context, they have been used as luminescent probes for one- or two-photon imaging,[3,4] as responsive probes able to detect and quantify in vitro or in cellulo biological activity or the presence of a given substrate (pH, metal ions, bicarbonate, lactate, urate)[5] and as emissive bioconjugated tags for time-resolved Förster resonance energy-transfer assays.[6]

[a] M. Soulié, F. Latzko, E. Bourrier, Dr. J. M. Zwier, Dr. L. Lamarque
Cisbio Bioassays, Parc Marcel Boiteux
BP 84175, 30200 Codolet (France)
E-mail: llamarque@cisbio.com

[b] Dr. V. Placide, Dr. P. L. Baldeck, Dr. C. Andraud, Dr. O. Maury
University of Lyon, ENS Lyon, CNRS-UMR 5182
46 Allée d'Italie 69364 Lyon (France)
E-mail: olivier.maury@ens-lyon.fr

[c] Dr. S. J. Butler, Dr. R. Pal, Dr. J. W. Walton, Prof. D. Parker
Department of Chemistry, Durham University
South Road, Durham, DH1 3LE (UK)
E-mail: david.parker@dur.ac.uk

[d] Dr. B. Le Guennic
Institut des Sciences Chimiques de Rennes, UMR 6226 CNRS
Université de Rennes 1
263 Avenue du Général Leclerc 35042 Rennes (France)

[e] Dr. P. L. Baldeck
Laboratoire de spectrométrie Physique Université Joseph Fourier
BP 87, 38402 Saint Martin d'Hères (France)

Supporting information for this article is available on the WWW under http://dx.doi.org/10.1002/chem.201402415.

The f-block elements exhibit intrinsic spectroscopic advantages for such applications. Their sharp emission bands and large pseudo-Stokes shifts following indirect ligand excitation facilitate selective detection in biological media even in a multiplexing experiment, and their long excited-state lifetimes enable time-resolved detection of the luminescence signal.[6c] These spectral and temporal resolutions result in a significant increase in signal-to-noise ratio, which is crucial for imaging purposes.[7]

All of these favorable properties have triggered the design of numerous complexes that meet a stringent set of requirements: 1) the complexes must be strongly coordinated to minimize nonradiative losses and ensure their stability in biological media, bearing in mind that coordinated water molecules are effective quenchers of the lanthanide excited state, 2) they must be sufficiently water soluble, and 3) they must have optimal brightness B ($B=\varepsilon\Phi$, where ε is the extinction coefficient and Φ the quantum yield) for enhanced detection, ideally at an excitation wavelength above 330–350 nm to allow the use of glass microscopy objectives. The choice of the chelating ligand and of the organic chromophore antenna modifies these requirements[8] and has led to the design of several classes of compounds, for example, cryptates,[9] helicates,[10] polyaminocarboxylates or -phosphinates,[11] and macrocyclic derivatives, including those based on the well-known cyclen family.[12] In this context, taking advantage of the established stability of lanthanide complexes of triazacyclononane tris-pyridine carboxylates[13] and (methyl/phenyl) phosphinates[14] ([Ln.**Lc**], [Ln.**Lmp**], and [Ln.**Lpp**], respectively; Figure 1), we recently reported ytterbium-based bioprobes for thick-tissue imaging by near-infrared two-photon microscopy[15] and excep-

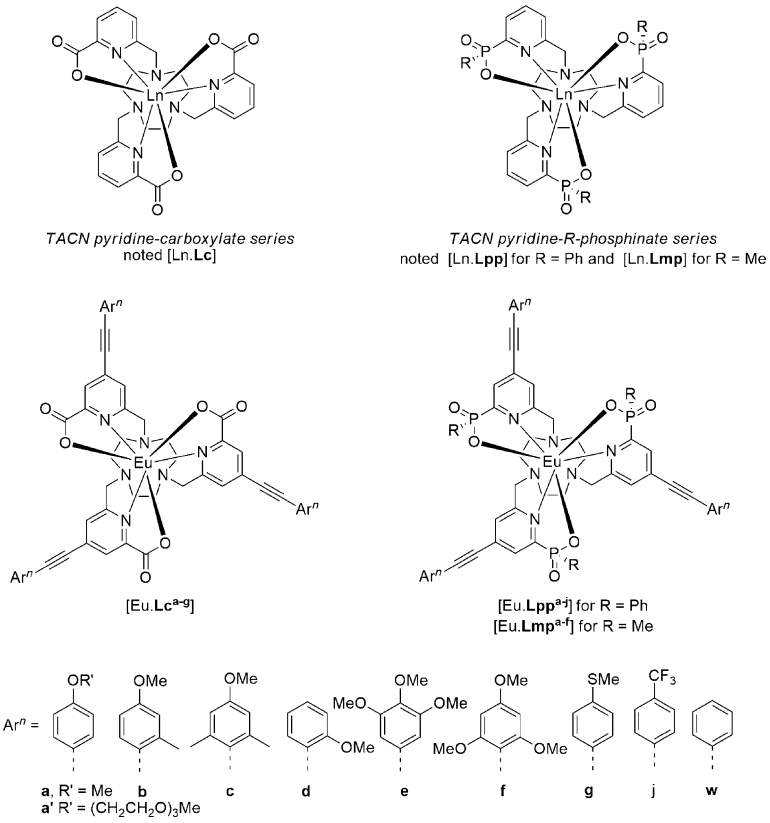

Figure 1. Structures of the complexes.

tionally bright europium-based bioprobes that can image cellular mitochondria and act as FRET donors ([Eu.**Lc**^{a}], [Eu.**Lmp**^{a}], and [Eu.**Lpp**^{a}]; Figure 1).[16] Their exceptional brightness of about 25 000 mol L^{-1} cm^{-1} on excitation at 340 nm is about one order of magnitude higher than those previously reported for europium complexes, and can be mainly explained by optimization of the extinction coefficient of the complex by using alkoxyphenylethynyl charge-transfer antennas.[17] In addition, europium complexes of heptadentate ligands featuring identical antennas have been reported to show additional sensing properties following displacement of the coordinated water molecule.[18]

The great potential of this series of complexes prompted us to gain further insight into the influence of the nature of the antenna on their luminescence properties. Herein, we report the synthesis and spectroscopic properties of a series of europium and terbium complexes featuring various antennas based on the same phenylethynyl scaffold. The nature, number, and position of electron-donating or electron-withdrawing aryl substituents was varied systematically (Figure 1), and the photophysical properties of [Eu.**Lc**^{a}], [Eu.**Lmp**^{a}], and [Eu.**Lpp**^{a}] are compared and discussed on the basis of their DFT calculated structures. Finally, the europium complexes were examined in cell-imaging applications, and selected terbium complexes were studied as potential oxygen sensors.

Results and Discussion

Synthesis

The synthesis of the 1,4,7-triazacyclononane (TACN) pyridine-carboxylate series is depicted in Scheme 1 and starts from the commercially available free aryl alkynes **1a**,**b**,**d** (X = H) or trimethylsilyl-protected derivatives **1e**,**g**, which were prepared according to literature procedures (see Supporting Information). Sonogashira palladium cross-coupling with pyridine derivative **2a** led to the chromophore scaffold in good yield. Chromophores **1e**,**g** were obtained by using a modified Sonogashira procedure with addition of tetrabutylammonium fluoride to the reaction mixture, which allows in situ deprotection of the trimethylsilyl group. Alternatively, we demonstrated that the trimethylsilyl alkyne moiety could be incorporated on the pyridine ring to give **2b** in 90% yield. However, due to the poor stability of the corresponding free alkyne **2c**, the desired compound was not obtained. We circumvented this issue by using the previous modified Sonogashira cross-coupling reaction leading to chromophore **3c**.

The starting material **1c** was readily available by alkylation of the corresponding iodophenol (see Supporting Information). Activation of alcohols **3** with mesyl chloride and purification on silica gel gave the corresponding mesylated compounds **4a**–**e**,**g**. Alkylation of TACN in the presence of potassium carbonate in acetonitrile gave rise to ligands **5a**–**e**,**g**, which were subsequently hydrolyzed, and the europium complexes were formed by addition of europium chloride hexahydrate. Each complex was isolated after purification by preparative HPLC and the structure confirmed by HRMS.

Details of the syntheses of **Lpp**^{a} and **Lpp**$^{a'}$ have been reported earlier.[16] The synthesis of the ligands **Lmp**^{b}, **Lmp**^{f}, and **Lpp**^{j} (Scheme 2) involved preparation of *p*-bromopyridyl phosphinate intermediates **2d**,**e**, which were elaborated to conjugated alkynyl chromophores **6b**,**f**,**j** in a Pd-catalyzed Sonogashira coupling reaction. Subsequent mesylation of the pyridyl alcohol, alkylation with TACN, and basic hydrolysis of the phosphinate ester groups provided the nonadentate ligands **Lmp**^{b}, **Lmp**^{f}, and **Lpp**^{j} in good yield over three steps.

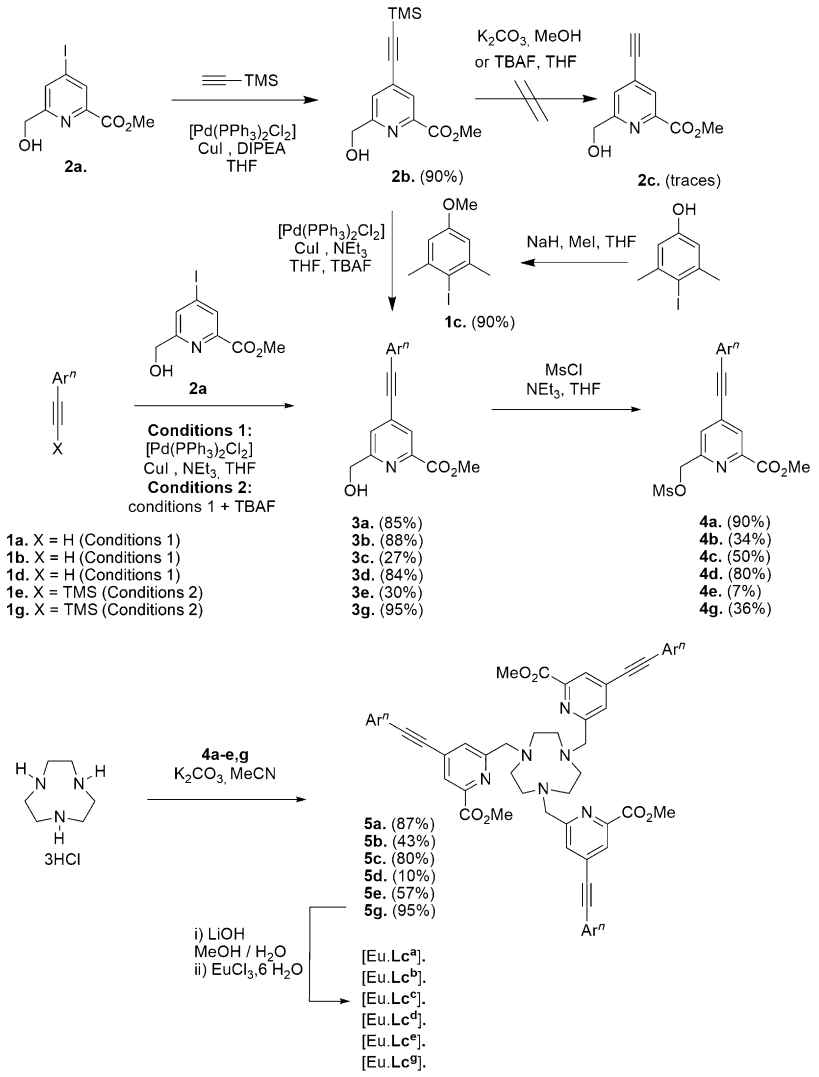

Scheme 1. Syntheses of the europium carboxylate series of complexes.

Structural comparison between [Eu.Lc[a]], [Eu.Lpp[a]], and [Eu.Lmp[a]]

DFT geometry optimizations were performed to evaluate the influence of the nature of the chelating arm, that is, carboxylate, methylphosphinate, or phenylphosphinate, on the coordination sphere of the complex (see Computational Details in Experimental Section). Model complexes [Y.**Lc**[a]], [Y.**Lmp**[a]], and [Y.**Lpp**[a]], in which the paramagnetic Eu^{III} ion was replaced by Y^{III}, were used to simplify the calculations.[19] Each complex adopts a helical structure with overall C_3 symmetry (Figure 2). The coordination polyhedron is a slightly distorted tricapped trigonal prism, composed of three nitrogen atoms of the TACN ring, three nitrogen atoms of the pyridine fragment (N_{py}), and three oxygen atoms from the carboxylate or phosphinate substituents. The calculated bond lengths and angles (Table 1) follow a similar trend to that observed in the X-ray structure of [Eu.**Lpp**[a]][16a] and related unsubstituted complexes.[13,14] The tetrahedral geometry around the phosphorus atom in complexes [Y.**Lpp**[a]]and [Y.**Lmp**[a]] imposes a smaller C_{py}-P-O angle of about 101° compared to the C_{py}-C-O angle of 112° in [Y.**Lc**[a]], and consequently the five-membered Y,N_{py},C_{py},P,O chelate ring is more constrained than that of the analogous carboxylate chelate (Y,N_{py},C_{py},C,O). These observations explain why the $Y–N_{py}$ distances are longer and why the central metal ion is more deeply encaged in the phosphinate complexes than in the carboxylate complexes, as illustrated by the variation of the distance *d* between the Y atom and the plane formed by the three nitrogen atoms of the TACN ring (Table 1). In addition, in the phosphinate complexes, the methyl or phenyl substituents of the phosphorus atom point along the C_3 axis and provide significant steric protection of the upper side of the complexes. Moreover, in the X-ray structure of [Eu.**Lpp**[a]], only one classical intermolecular π–π interaction is found in the lattice, and it involves the phenylphosphinate rings and not the alkynyl moieties. The centroid–centroid distance is 4.07 Å, with the two phenyl rings shifted by 1.90 Å from perfect stacking.

Photophysical properties of Eu complexes

Comparison between Lc, Lmp, and Lpp ligands

The photophysical properties of the complexes were studied in dilute methanol solution or in water, and representative data are reported in Table 2. The absorption and emission spectra of [Eu.**Lc**[a]], [Eu.**Lmp**[a]], and [Eu.**Lpp**[a]], which feature identical antennas but different chelating groups, are compared in Figure 3. In the absorption spectra, each complex has a broad structureless transition, assigned to an intraligand charge-transfer (ICT) transition from the electron-donating methoxyphenyl group(s) to the electron-withdrawing pyridine fragment. Interestingly, the absorption of [Eu.**Lc**[a]] is slightly redshifted compared to the phosphinate analogues, in terms of both the maximal absorption wavelength ($\Delta\lambda_{max}=8$ nm) and the red tail of the absorption band ($\Delta\lambda_{cutoff}=20$ nm). This bathochromic shift can be explained by the shorter $Ln–N_{py}$ distance observed for the carboxylate compound: a shorter distance leads to stronger coordination of the metal center, the

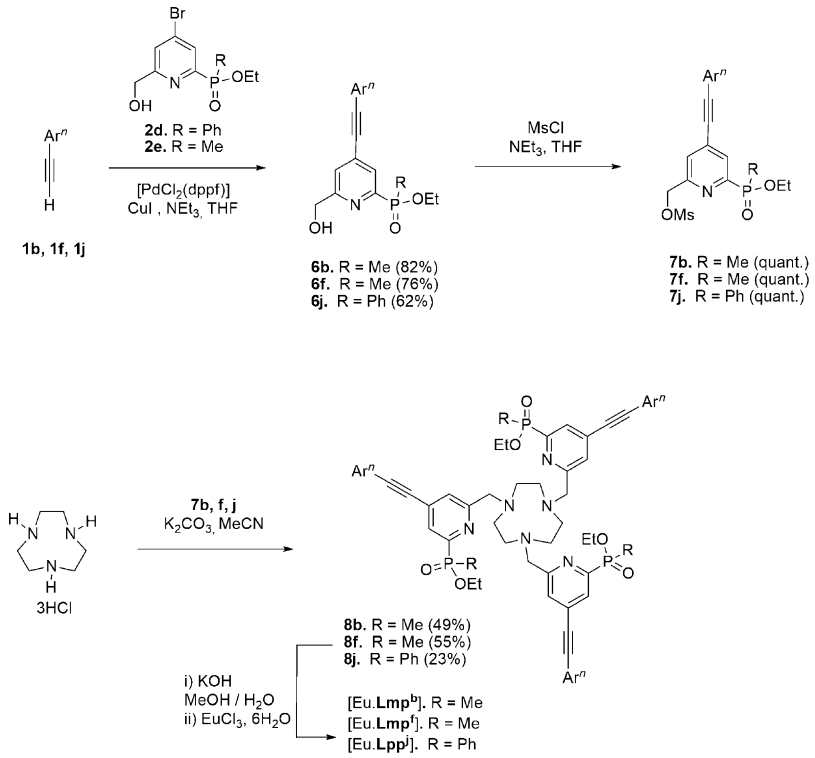

Scheme 2. Syntheses of the europium phosphinate series of complexes.

Lewis acidity of which enhances the accepting character of the pyridine fragment.

The europium emission spectral profiles are very similar for each complex (Figure 3), with a hypersensitive $\Delta J = 2$ transition around 610–620 nm, as expected for threefold-symmetric compounds incorporating polarizable donor groups. A small increase in the intensity of the $\Delta J = 4$ transition around 680–700 nm was observed for [Eu.**Lmp**^{a}] and [Eu.**Lpp**^{a}] compared to [Eu.**Lc**^{a}], which may be tentatively associated with increasing distortion from the ideal C_3 symmetry in the case of the more bulky phosphinate derivatives. Remarkable quantum yields in MeOH of 42, 43, and 52% were found for [Eu.**Lc**^{a}], [Eu.**Lmp**^{a}], and [Eu.**Lpp**^{a}], respectively (Table 2). In addition, in water the quantum yield of [Eu.**Lmp**^{a}] is almost conserved (39%), whereas it drops to 25% for [Eu.**Lc**$^{a'}$], the water-soluble analogue of [Eu.**Lc**^{a}]. Such behavior is in agreement with the increased steric protection afforded by the methyl or phenyl substituents at the phosphorus atom (Figure 2).

To gain deeper insight into the influence of the nature of the coordinating group, the relevant radiative and nonradiative parameters were deduced from experimental data (spectra, quantum yields, and lifetimes). By using the approach initially proposed by Werts, Jukes, and Verhoeven[20] and Beeby et al.[21] the overall quantum yield of europium luminescence ϕ_{Eu} is defined as the product of the efficiency of sensitization η_{sens} (i.e.,

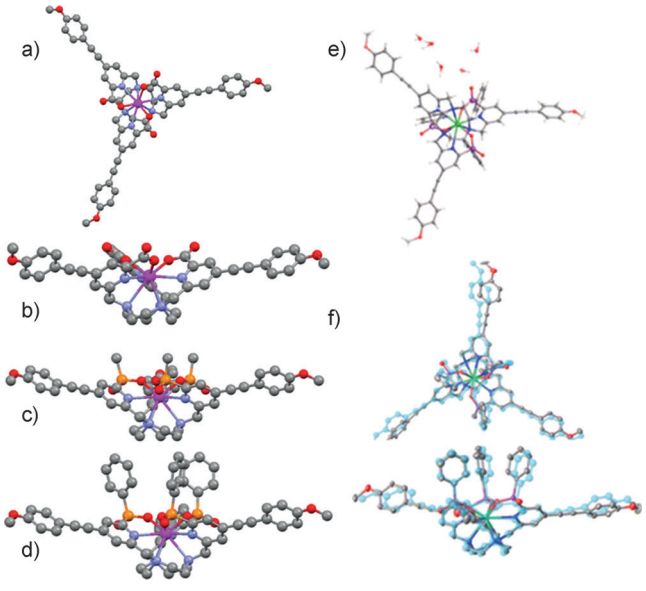

Figure 2. DFT-optimized structure of [Y.**Lc**^{a}] (a, b), [Y.**Lmp**^{a}] (c), and [Y.**Lpp**^{a}] (d) with the C_3 symmetry axis perpendicular (a) or parallel (b–d) to the plane of the figure. Atom colors: C gray, N blue, O red, P orange, Y magenta. Hydrogen atoms have been omitted for clarity. e) X-ray structure of [Eu.**Lpp**^{a}].[16a] f) Correspondence between X-ray (bold) and DFT (ghost) structures.

Table 1. Optimized DFT distances [Å] and angles [°] for the series of Y^{III} model complexes.

	[Y.**Lc**^{a}]	[Y.**Lmp**^{a}]	[Y.**Lpp**^{a}]
Y–N	2.829/2.830/2.831	2.787/2.787/2.787	2.768/2.768/2.769
Y–N_{py}	2.563/2.563/2.564	2.703/2.700/2.703	2.676/2.676/2.676
Y–O	2.246/2.247/2.247	2.214/2.214/2.215	2.213/2.214/2.213
d	2.250	2.190	2.170
N-Y-N	63.4/63.4/63.3	64.7/64.7/64.7	65.0/65.0/65.0
N_{py}-Y-N_{py}	119.8/119.8/119.6	119.7/119.7/119.7	119.8/119.8/119.8
O-Y-O	94.5/94.3/94.3	91.4/91.5/91.5	89.8/89.8/89.8
N-Y-O[a]	120.0/119.9/120.1	122.3/122.3/122.3	123.6/123.6/123.6

[a] Intraligand angle.

Table 2. Calculated values of τ_r, k_r, and Σk_{nr} for [Eu.**Lc**^{a}], [Eu.**Lmp**^{a}], and [Eu.**Lpp**^{a}] in methanol by using the room-temperature experimentally determined quantities τ_{obs} and $[I(0,1)/I_{tot}]$.

Complex	$I(0,1)/I_{tot}$	τ_{obs} [ms]	τ_r [ms]	k_r [s^{-1}]	Σk_{nr} [s^{-1}]
[Eu.**Lc**^{a}]	0.087	0.99	2.72	368	642
[Eu.**Lmp**^{a}]	0.079	1.18	2.47	405	443
[Eu.**Lpp**^{a}]	0.086	1.30	2.68	473	396

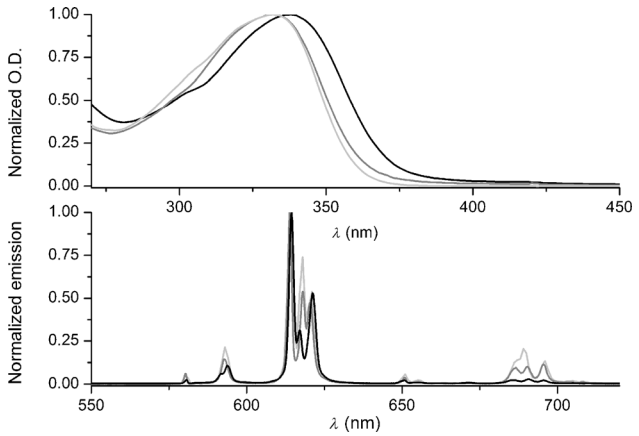

Figure 3. Comparison of the absorption (top) and emission (bottom) spectra of [Eu.**Lc**^{a}] (black), [Eu.**Lmp**^{a}] (gray), and [Eu.**Lpp**^{a}] (light gray) in methanol at room temperature ($\lambda_{ex}=340$ nm).

Table 3. Spectroscopic properties of the complexes measured at room temperature in MeOH.

Complex	λ_{max} [nm]	ε [mM^{-1}cm^{-1}]	ϕ [%][a,b]	τ [ms]	σ_{TPA} (at 700 nm)[b]
[Eu.**Lc**^{a}]	339	58 000	42	0.99	46
[Eu.**Lc**^{b}]	345	60 000	55	0.97	
[Eu.**Lc**^{c}]	351	60 000	45	0.90	
[Eu.**Lc**^{d}]	339	60 000	41	1.01	30
[Eu.**Lc**^{e}]	341	60 000	8	0.49	36
[Eu.**Lc**^{g}]	349	60 000	32	0.85	
[Eu.**Lc**^{w}][c]	315[c]	48 400[c]	22[c]	0.85[c]	
[Eu.**Lpp**^{a}]	332	58 000	52	1.30	26
[Eu.**Lmp**^{a}]	331	58 000	43	1.18	
[Eu.**Lmp**^{b}]	340	62 000	54	1.14	
[Eu.**Lmp**^{f}]	360	57 000	55	1.05^{c}	

[a] Quinine sulfate as standard, excitation at 335 nm, errors in quantum yield or lifetime are ±15%. [b] Errors are ±20%. [c] Data recorded in water according to Ref. [13a].

the fraction of energy transferred from the donor state to the Eu^{III} accepting levels) and the quantum efficiency of the metal-centered luminescence on direct excitation into the f levels η_{Eu} [Eq. (1)]

$$\phi_{Eu} = \eta_{sens}\eta_{Eu} \quad (1)$$

in which $\eta_{Eu}=\tau_{obs}/\tau_r$ where τ_{obs} is the experimental luminescence lifetime of the complex and τ_r the pure radiative lifetime [Eq. (2)]

$$k_r = 1/\tau_r = A(0,1)[I_{tot}/I(0,1)] \quad (2)$$

where the constant $A(0,1)$ is the spontaneous emission probability of the $^5D_0\rightarrow{}^7F_1$ transition (32 s^{-1} in methanol) and $I_{tot}/I(0,1)$ the ratio of the total integrated emission intensity to the intensity of the $^5D_0\rightarrow{}^7F_1$ transition. Finally, if k_r and τ_{obs} are known, the nonradiative decay rate constant Σk_{nr} can be deduced from Equation (3).

$$\Sigma k_{nr} = 1/\tau_{obs} - 1/\tau_r \quad (3)$$

This procedure was used for [Eu.**Lc**^{a}], [Eu.**Lmp**^{a}], and [Eu.**Lpp**^{a}] in methanol, and the data are summarized in Table 2. Clearly, the increases in quantum yield and experimental lifetime along the series [Eu.**Lc**^{a}] < [Eu.**Lmp**^{a}] < [Eu.**Lpp**^{a}] are directly connected to the strong decrease of the nonradiative rate constant from 642 to 396 s^{-1}. These results clearly indicate that the increased steric protection afforded by the phosphinate substituent (Me < Ph) contributes strongly to rigidification of the structure of the complex, and thereby reduces nonradiative de-excitation pathways.[14b]

Influence of alkynyl substitution

The influence of the aromatic substitution on the photophysical properties (absorption and emission) of the related europium(III) complexes was thoroughly studied. Table 3 compiles the spectroscopic data of compounds [Eu.**Lc**$^{a-g}$] alongside data for the unsubstituted compound [Eu.**Lc**^{w}] for comparison. The absorption spectrum of [Eu.**Lc**^{w}] shows a structured transition with a maximum at 315 nm ($\lambda_{cutoff}=335$ nm) characteristic of a π–π* transition associated with a local excited state ^{1}LE (Figure 4).[22] As expected, substitution of the aromatic moiety by electron-donating groups, for example, OMe and SMe in [Eu.**Lc**$^{a-g}$], induces a profound modification of the absorption spectra with the appearance of a broad structureless transition assigned, by comparison with analogous ligands,[9c,17] to an ICT transition. These ICT transitions are bathochromically shifted, and the magnitude of the redshift ($\Delta^{a-g}=\lambda$([Eu.**Lc**$^{a-g}$])−λ([Eu.**Lc**^{w}]) is correlated to the strength of the donating groups. As a consequence of the stronger donor character of the SMe group compared to OMe, $\Delta^{g}=34$ nm is higher than $\Delta^{a,d}=19$ nm for one methoxyl substituent in *para* or *ortho* position, respectively. Introduction of additional methoxyl groups in the nonconjugated *meta* position does not induce any significant

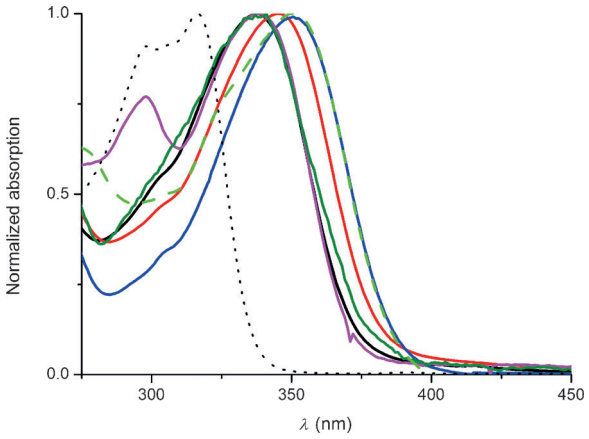

Figure 4. Normalized absorption spectra of complexes [Eu.**Lc**$^{a-w}$] in dilute methanol solution (black dotted [Eu.**Lc**^{w}]; black [Eu.**Lc**^{a}]; red [Eu.**Lc**^{b}]; blue [Eu.**Lc**^{c}]; pink [Eu.**Lc**^{d}]; olive [Eu.**Lc**^{e}]; green dashed [Eu.**Lc**^{g}]).

additional bathochromic shift ($\Delta^{e} = 21$ nm). On the contrary, introduction of one or two weakly electron-donating methyl groups in the *ortho* position induces additional redshifts of 30 and 36 nm for [Eu.**Lc**^{b}] and [Eu.**Lc**^{c}], respectively. Finally, introduction of three methoxyl groups in conjugated *ortho*, *ortho*′, and *para* positions in [Eu.**Lmp**^{f}] results in the strongest bathochromic shift of the ICT transition, with a maximal absorption wavelength of 360 nm and a λ_{cutoff} value of about 410 nm. It is therefore possible to fine-tune the maximum absorption wavelength and the cutoff wavelength in the spectral range of interest centered around 337 nm by varying the aromatic substitution. This ICT transition is very intense, with an extinction coefficient of about 60000 L mol^{-1} cm^{-1} and thus of prime importance in terms of brightness optimization. All compounds except [Eu.**Lc**^{e}] are strongly emissive and exhibit the classical Eu^{III} emission profile on irradiation in the ICT transition. In each case, no residual ligand-centered emission was observed, that is, the energy transfer to the lanthanide ion is almost quantitative. The quantum yields in methanol are good to excellent, and the highest value of 55% was obtained for [Eu.**Lc**^{b}] and [Eu.**Lmp**^{f}], supported by long luminescence lifetimes around 1 ms. The photophysical properties of all complexes were not evaluated in water due to their limited solubility, except for [Eu.**Lmp**^{a}]. The quantum yield (39%) and lifetime (1.01 ms) in water are slightly lower than in methanol but remain significant and indicate good aqueous stability of this complex. Combined with the above-mentioned strong absorption, this family of complexes exhibits very high brightness around 337 nm, which makes them very attractive candidates for bioimaging and fluoroimmunoassay applications.

Sensitization process

In related tris-dipicolinate complexes, europium sensitization has been shown to occur by an efficient intramolecular energy-transfer process involving a relaxed and fairly broad ICT excited state and not via a localized ligand triplet state, notably for strongly electron donating moieties.[17b] In the case of weak donor groups such as alkyl and alkoxyl, the ICT state lies at higher energy, and consequently a contribution of the classical triplet-mediated sensitization process remains possible.[17a]- Complexes [Gd.**Lmp**^{f}] and [Gd.**Lpp**$^{a'}$] were prepared and investigated in order to study the influence of the chelating groups on the sensitization process (Figure 5). At low temperature, both complexes exhibit a broad structureless emission, characteristic of an ICT state, at 415 and 375 nm for [Gd.**Lmp**^{f}] and [Gd.**Lpp**$^{a'}$], respectively, together with weaker structured emission from the ligand-centered triplet state (e.g., vibrational overtones at 490 and 470 nm). At room temperature, only a broad structureless ICT emission is observed around 460 nm. This variable-temperature measurement clearly indicates the presence of a triplet excited state at approximately the same energy as the ICT state. Consequently, the two sensitization pathways, that is, the triplet-state-mediated and direct ICT processes, can be simultaneously involved in the sensitization of europium luminescence.

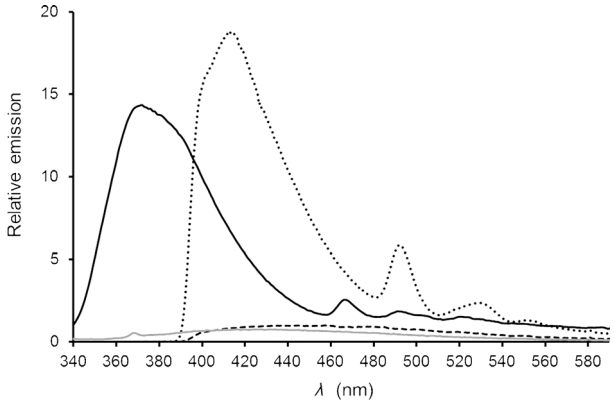

Figure 5. Emission spectra of [Gd.**Lmp**^{f}] ($\lambda_{exc} = 355$ nm) measured at 77 K (black dotted) and 295 K (black dashed), as well as [Gd.**Lpp**$^{a'}$](λ_{exc} 330 nm) at 77 K (black) and 295 K (gray). Recorded in an EPA glass .

The parent Eu^{III} complexes did not show significant spectral variation with solvent polarity, except for the Eu complex of the 2,4,6-trimethoxyphenyl triphosphinate ligand **Lmp**^{f}. In this case, the emission intensity increased in less polar solvents (Table 4 and Figure S1 in the Supporting Information). In solvents with a Reichardt normalized polarity parameter $E_T(30)$ of less than 0.8 (e.g., MeOH, EtOH, *i*PrOH, MeCN, DMF) the lifetime increased slightly from 1.06 in MeOH to 1.18 in *i*PrOH. Based on the assumption that the extinction coefficients of the lowest-energy ICT band do not vary by more than 10% in the examined solvents, the overall emission quantum yield varied from 55% in MeOH to 78% in *i*PrOH. However, in water the lifetime was 0.70 ms, the quantum yield dropped to 5%, and the primary absorption band of the ICT state broadened and extended beyond 405 nm.

Table 4. Variation of spectral behavior with solvent polarity for [Eu.**Lmp**^{f}].

Solvent	$E_T(30)$	λ_{max} [nm]	τ [ms]	I_{rel} [%][a]
water	1.00	360	0.72	10
MeOH	0.76	360	1.06	55
EtOH	0.65	360	1.15	71
*i*PrOH	0.55	360	1.18	78
MeCN	0.46	350	1.17	81
DMF	0.40	350	1.17	75

[a] Relative emission intensities were estimated under the assumption that the extinction coefficient of [Eu.**Lmp**^{f}] is the same in each solvent and were calibrated with the quantum yield in MeOH; prior work has shown that for water and methanol, the ICT extinction coefficients of the lowest-energy band are very similar, within an error of ±10%.

The variation of the emission intensity with T in the range 180–295 K was examined in EPA (diethyl ether/isopentane/ethanol 5/5/2 v/v/v), and the changes in intensity and lifetime with oxygen partial pressure p_{O_2} in the range 0.4—160 mmHg was examined in water at ambient temperature. The temperature variation was characterized by an increase in overall emission intensity by a factor of two between 295 and 230 K fol-

lowed by a drop in intensity at much lower temperatures (Figure S2 in the Supporting Information). The emission intensity varied nonlinearly (Figure S3 in the Supporting Information) with p_{O_2} below 35 mmHg (160 mmHg is atmospheric pressure), with a 2.6-fold increase in intensity at 0.4 mmHg with respect to ambient pressure.

Taken together, the absorption-, solvent-, temperature-, and oxygen-dependent changes observed for [Eu.**Lmp**^{f}] support a sensitization mechanism involving a solvent-relaxed ICT excited state, which may transfer its energy to the Eu $^5D_1$ and/or $^5D_0$ excited states. The energy of this ICT excited state is lowered in the most polar solvent water, such that thermally activated (*T*-dependent) back energy transfer may occur, which extends the lifetime of the ICT state and thereby increases its sensitivity to nonradiative deactivation.

Nonlinear optical properties

The presence of the extended π-conjugated antenna ligand prompted us to determine the two-photon absorption cross sections of selected complexes. To that end, two-photon excited fluorescence (TPEF) measurements, based on the calibration of the two-photon excitation spectra in the range 700–900 nm, were performed in dilute methanol solution by using coumarin 307 as external reference (see Experimental Section for details). The two-photon absorption spectra are shown in Figure 6, and it clearly appears that the maximal absorption

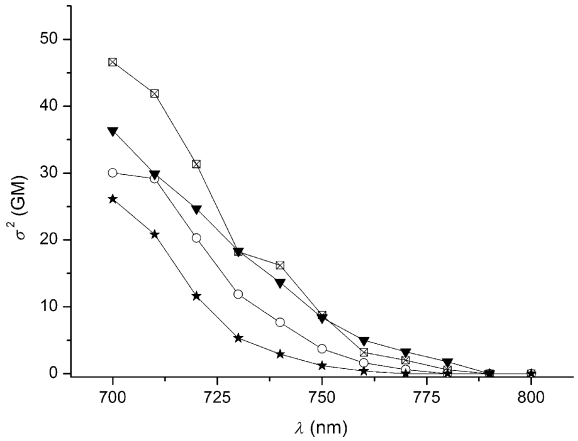

Figure 6. Two-photon absorption measured by TPEF in methanol of [Eu.**Lc**^{a}] (empty squares), [Eu.**Lc**^{d}] (empty circles), [Eu.**Lc**^{e}] (filled triangles), and [Eu.**Lpp**^{a}] (filled stars).

wavelength is located out of our laser excitation range and that only the red tail of the two-photon absorption spectrum can be measured. At 700 nm, all compounds show rather modest two-photon absorption cross sections of between 25 and 50 GM; these values lie in the range of those of recently described complexes with similar antenna groups.[4a,9c,17,23] Such properties render this family of complexes suitable for biphotonic microscopy imaging applications.

Bioimaging application: mitochondrial staining in different cell types

In a preliminary communication, we reported that certain Eu complexes in this family exhibit cell uptake, with a tendency to highlight the mitochondrial network.[14a] Indeed, it was possible to obtain both single- (λ_{exc} = 355, 365 nm) and two-photon (λ_{exc} = 710–730 nm) microscopy images with several of the complexes described herein.[24] The single-photon images are representative and are described here. The high optical brightness of the probes allows live-cell imaging at high resolution (Figure 7). Thus, in the case of mouse skin fibroblasts (NIH-3T3)

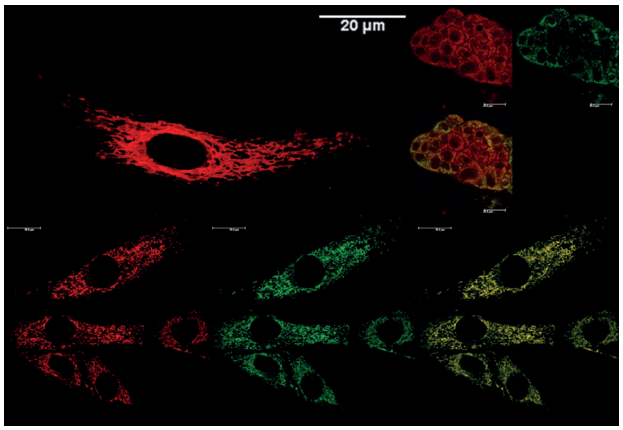

Figure 7. Top left: NIH 3T3 cells stained with [Eu.**Lmp**^{b}], clearly showing the mitochondrial network at high resolution (recorded with an in-house phase-modulation nanoscope: 2048×2048 pixels, voxel size 60×60×780 nm). Top right: [Eu.**Lmp**^{f}] in HepG2 cells (which tend to clump together, forming local foci during culturing) in red, showing higher definition and resolution compared to images with MitoTracker Green, and a co-localized image. Bottom: [Eu.**Lmp**^{f}] (30 μM loading concentration) in NIH 3T3 cells (left, 2 h loading; 30 min for MTG, middle), showing the colocalization (right) with MTG images by RGB merge ($P > 0.9$; 1024×1024 pixels, voxel size 120×120×780 nm, 100 Hz, four scans averaged).

stained with [Eu.**Lmp**^{b}] or [Eu.**Lmp**^{f}], their high brightness permits use of a new experimental technique, which can be termed phase-modulated nanoscopy, to further reduce lateral resolution (d_{lat} = 125 nm at λ_{exc} = 355 nm, 1.4 N.A.).[16] This is revealed in the definition of the mitochondrial network down to about 80 nm resolution.

The complex [Eu.**Lmp**^{f}] absorbs even more strongly at 355 nm and was also examined in human liver adenocarcinoma cells (HepG2), where it revealed the mitochondrial distribution better than the common stain MitoTracker Green (MTG). These liver cells form defined local foci instead of a well-dispersed monolayer. Therefore, we conducted a simple comparison of the tissue penetration of [Eu.**Lmp**^{f}] versus MTG. This Eu complex appears to permeate the foci more deeply, allowing more effective visualization of the taller axial sections of these densely packed cells. Following uptake through macropinocytosis,[25] the complex must be shuttled to the mitochondria, crossing the outer membrane and becoming localized in the intermembrane space. It seems unlikely that these high molecular weight ($M > 500$) probes can cross the inner mitochondrial

membrane. Such behavior may then explain their low mitochondrial toxicity, as revealed by IC_{50} values of greater than 100 μM (24 h) in the MTT assay. The MitoTracker stains are based on substituted benzylic chlorides that irreversibly alkylate Cys residues in various mitochondrial proteins (e.g., heat shock protein 60, VDAC1, aldolase A)[26] and can also attack mitochondrial DNA by alkylation at guanine N-7. These reactions result in irreversible perturbation of normal organelle function, so that these organic dyes can only penetrate and stain the outer layers of the foci and subsequently form a perturbed cell barrier. These shallow superficial stained cell layers appear to prevent penetration and transport of the organic dye deeper into the tissue. Also, it can be clearly seen in the sets of images in HepG2 cells (Figure 7), that the Eu compound does not stain the lipid droplets that appear as very bright spots in the images obtained with the organic dye.

Photophysical properties of terbium complexes

The effect of changing the nature of the *para* substituent on the phenyl ring was considered in an attempt to make this ligand suitable for terbium sensitization. This strategy requires raising of the energy of the ligand singlet excited state and/or the relative energy of the ICT and ligand-centered triplet states. Earlier work[27] has shown that very little terbium emission was observed under ambient conditions for complexes of the ligands with chromophores bearing electron-releasing substituents, for example, **Lc**[a] and **Lpp**[a]. Even in deoxygenated solution, [Tb.**Lpp**[a]] gave only very weak emission (ϕ_{em}(MeOH) = 0.3% at 295 K, Figure S4 in the Supporting Information). Sensitization is much less likely to occur with the terbium analogues, as the Tb ion requires that the broad ICT state lie well above the terbium $^5D_4$ accepting state at 20400 cm^{-1}. Indeed, sensitization of terbium in the near-UV region by an antenna normally requires that a significant energy gap between the energy of the excited state of the sensitizing moiety and the accepting Tb $^5D_4$ level.[8] In this situation, the rate of thermally activated back energy transfer is minimized when the energy gap is less than 8*kT*, that is, 1640 cm^{-1} at 298 K. In an effort to identify a system that may allow Tb sensitization with reduced or zero oxygen sensitivity, the excited-state energies of a set of chromophores **9b**–**e** with electron-poor substituents were measured (Scheme 3, Table 5, and Figure 8).

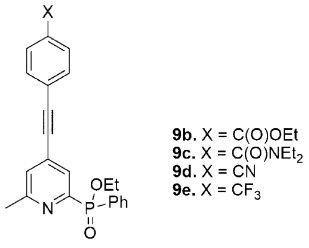

9b. X = C(O)OEt
9c. X = $C(O)NEt_2$
9d. X = CN
9e. X = CF_3

Scheme 3. Structure of phenylphosphinate model chromophores **9b**–**e** featuring electron withdrawing substituents.

Table 5. Selected photophysical properties for phenylphosphinate-based pyridyl-alkynyl chromophores **9b**–**e** (295 K, MeOH, or as stated).

Compound	Substituent X	λ_{max} [nm]	ε [$mM^{-1}cm^{-1}$][a]	E_T [cm^{-1}][b]
[Gd.**Lpp**[a]]	$(OCH_2CH_2)_3OMe$	320	25000	21300
9b	$CO_2CH_2CH_3$	314	31800	21200
9c	$CON(CH_2CH_3)_2$	310	34600	21,600
9d	CN	312	33500	21000
9e	CF_3	298	15000	21800

[a] Errors are ±5%. [b] Triplet energies E_T were measured at 77 K in an EPA glass.

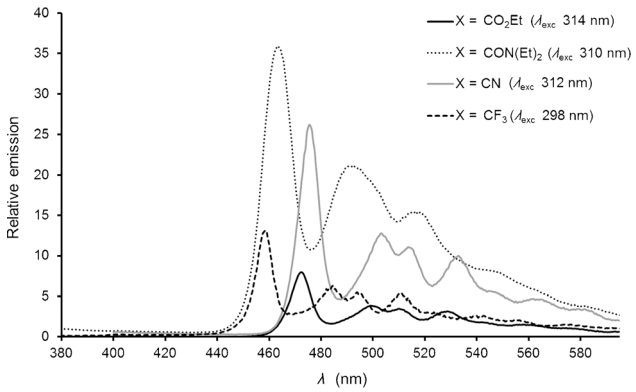

Figure 8. Phosphorescence emission spectra of a series of phenylphosphinate model chromophores **9b**–**e** measured in an EPA glass at 295 K.

Oxygen sensing with Eu/Tb mixtures

The *p*-CF_3-substituted chromophore has the highest triplet energy of this series. Indeed, the low-*T* spectra show that the triplet excited state is of lower energy than the ICT state in this case. Accordingly, the corresponding ligand **Lpp**[j] was prepared and the spectral properties of the Tb and Eu complexes analyzed in the presence of varying partial pressures of oxygen. The Eu complex showed no change in intensity as p_{O_2} was varied, whereas the Tb analogue exhibited a strong dependence on dissolved oxygen concentration (Figure 9). The emission intensity of Tb was assessed over the p_{O_2} range of 0.03 to 159 mmHg and showed a linear dependence, associated with a Stern–Volmer quenching constant K_{SV}^{-1} of 60 mmHg. The differing behavior of the Eu and Tb complexes allows oxygen concentrations to be measured by determining the ratio of the green Tb emission at 545 nm to the red Eu emission at 620 nm for 1/10 mixtures of the Eu/Tb complexes (Figure 10). Such behavior has previously been observed for related systems[27] in which reversible energy transfer repopulates the sensitizer triplet excited state and renders it sensitive to collisional quenching by triplet oxygen.

Conclusion

We have developed a modular and flexible synthetic route to a family of ligands based on TACN that enables control of ligand and complex absorbance in the range 330–360 nm by variation of the substituents on the aryl ring or by changing

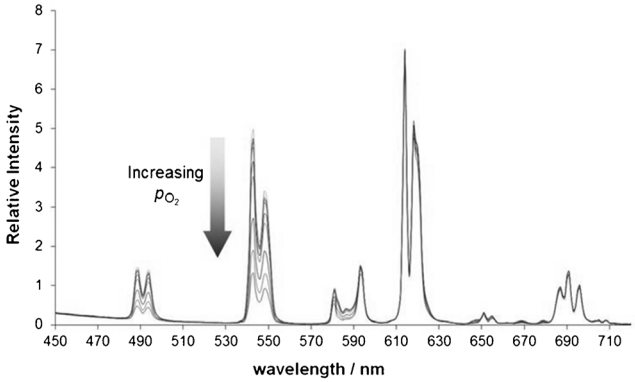

Figure 9. Emission spectra of the mixture of complexes [Ln.**Lpp**^{j}] (Eu/Tb = 1/10, λ_{exc} = 308 nm) showing the change in the $\Delta J = -1$ Tb emission-band intensity (centered at 545 nm) compared to the $\Delta J = 2$ Eu band (centered at 615 nm) as the atmospheric pressure (and hence the concentration of dissolved molecular oxygen) was varied from 2 to 760 mmHg.

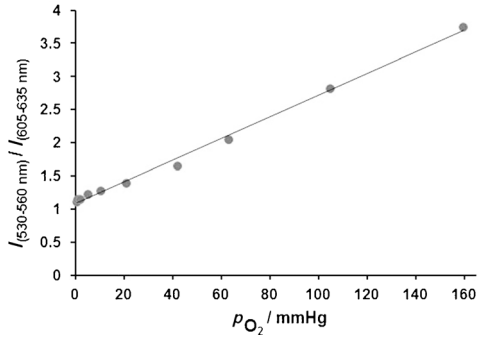

Figure 10. Variation of the ratio of the terbium emission intensity (λ_{exc} = 308 nm, λ_{em} = 530–560 nm) for [Tb.**Lpp**^{j}] versus Eu emission of [Eu.**Lpp**^{j}] as a function of p_{O_2} in aqueous solution (295 K).

the nature of the donor anionic group, as exemplified by the behavior of carboxylate and phosphinate groups. The phosphinate substituents were shown by DFT and X-ray studies to present a steric shield that protects the lower face of the lanthanide complexes, enhancing their resistance to collisionally activated quenching processes and leading to longer excited-state lifetimes.

The europium complexes showed both high emission quantum yields and high absorbance, which led to several examples having brightness B on the order of 15 to 30 $mM^{-1}cm^{-1}$, the highest reported for Eu complexes in solution. This high brightness permits applications in immunoassays and in single-photon microscopy and spectral imaging that are otherwise limited to longer acquisition times or higher complex concentrations, and it enables live cell imaging at low incident powers. Furthermore, the two-photon cross sections of the chromophores, which lie in the range 30–50 GM, are sufficient to allow excitation between 700 and 720 nm, as needed for two-photon microscopy studies. These studies, in concert with applications to near-IR emitting systems, will be discussed in forthcoming work.

The mechanism of sensitization involves a relaxed ICT excited state or a ligand triplet intermediate, depending on the nature of the aryl substituents and the donor group. Very efficient intramolecular energy transfer occurs with the Eu^{III} complexes, whereas for the Tb^{III} analogues, back energy transfer occurs rapidly in all cases, due to the broad density of states or the relatively low energy of the triplet or relaxed ICT excited state and their closeness to the terbium $^5D_4$ emissive state. By using a mixture of Tb and Eu complexes of a common ligand, the ability to measure p_{O_2} in solution was demonstrated.

Experimental Section

Computational details

DFT geometry optimizations of the Y^{III} complexes were carried out with the Gaussian 09 (revision A.02) package[28] by employing the PBE0 hybrid functional.[29]The Stuttgart/Dresden basis sets and effective core potentials were used to describe the yttrium atom,[30] whereas all other atoms were described with the SVP basis sets.[31]

Optical measurements

Absorption spectroscopy: UV/Vis absorption measurements were recorded on a JASCO V670 or a PerkinElmer Lambda 900 absorption spectrophotometer by using matched quartz cells.

Luminescence: Emission spectra were measured on a Horiba-Jobin Yvon Fluorolog-3 spectrofluorimeter. The steady-state luminescence was excited by unpolarized light from a 450 W xenon CW lamp and detected at an angle of 90° for dilute-solution measurements (10 mm quartz cell) by a red-sensitive Hamamatsu R928 photomultiplier tube. Spectra were reference-corrected for both the variation in intensity of the excitation source light (lamp and grating) and the emission spectral response (detector and grating). Phosphorescence lifetimes (> 30 μs) were obtained by pulsed excitation with a FL-1040 UP Xenon Lamp. Luminescence decay curves were fitted by least-squares analysis with Origin. Luminescence quantum yields Q were measured in dilute aqueous solutions with an absorbance of less than 0.1 by using the equation $Q_x/Q_r = [A_r(\lambda)/A_x(\lambda)][n_x^2/n_r^2][D_x/D_r]$, where A is the absorbance at the excitation wavelength λ, n the refractive index, D the integrated luminescence intensity, and "r" and "x" stand for reference and sample. The reference was quinine bisulfate in 1 N aqueous sulfuric acid solution ($Q_r = 0.546$). Excitation of reference and sample compounds was performed at the same wavelength.

Two-photon-excited luminescence measurements: The TPA cross-section spectrum was obtained by upconversion luminescence with a Ti:sapphire femtosecond laser in the range 700–900 nm. The excitation beam (5 mm diameter) was focused with a lens (focal length 10 cm) at the middle of the 10 mm cell. Emitted light was collected at 90° and was focused into an optical fiber (diameter 600 μm) connected to an Ocean Optics S2000 spectrometer. The incident beam intensity was adjusted to 50 mW to ensure an intensity-squared dependence of the luminescence over the whole spectral range. The detector integration time was fixed to 1 s. Calibration of the spectra was performed by comparison with the published 700–900 nm two-photon absorption spectrum of Coumarin 307 (quantum yield = 0.56 in ethanol).[32] The measurements were done at room temperature in dichloromethane and at a concentration of 10^{-4} M.

Variable-temperature (VT) and variable-pressure (VP) experiments: Details of the experimental setups used in the VT and VP experiments have been reported earlier.[27]

Confocal microscopy: Details of cell culture, epifluorescence microscopy, and assessment of complex toxicity, typically by using the MTT assay of mitochondrial redox function, have been reported elsewhere.[16]Cell images and co-localization experiments were performed with a Leica SP5 II microscope. To achieve excitation with maximal probe emission, the microscope was coupled by an optical fiber to a Coherent 355 nm CW (Nd:YAG) laser, operating between 4 and 8 mW power. A HeNe or Ar ion laser was used when commercially available organelle-specific stains (e.g., MitoTracker Green) were used to corroborate cellular compartmentalization. The microscope was equipped with a triple-channel imaging detector, comprising two conventional PMT systems and a HyD hybrid avalanche photodiode detector. The latter part of the detection system, when operated in the BrightRed mode, is capable of improving imaging sensitivity above 550 nm by 25% and reducing signal-to-noise ratio by a factor of 5. The pinhole was always determined by the Airy disk size, calculated from the objective in use (HCX PL APO 63×/1.40 N.A. LbdBlue) at the lowest excitation wavelength (355 nm). Scanning speed was adjusted to 100 Hz in a unidirectional mode to ensure both sufficient light exposure and enough time to collect the emitted light from the lanthanide-based optical probes (1024×1024 frame size, pixel size of 120× 120 nm, and depth of 0.772 μm).

Synthesis

Details of general methods and of NMR and MS instrumentation can be found in recent references.[2,4,7,8,16]. Experimental details of syntheses of chromophores, ligands, and complexes are given in the Supporting Information.

CCDC-857545 ([Eu.**Lpp**^{a}]) contain the supplementary crystallographic data for this paper. These data can be obtained free of charge from The Cambridge Crystallographic Data Centre via www.ccdc.cam.ac.uk/data_request/cif.

Acknowledgements

We thank EPSRC, the Royal Society, and the ERC for support (D.P., R.P., S.J.B.: FCC 266804); V.P. thanks the Lyon Science Transfer Agency for financial support.

Keywords: imaging agents · lanthanides · macrocyclic ligands · photophysics · sensors

[1] a) S. V. Eliseeva, J.-C. G. Bünzli, in *Springer series on fluorescence, Vol. 7, Lanthanide spectroscopy, Materials, and Bio-applications, Vol. 1* (Eds.: P. Hännen, H. Härmä), Springer, Berlin, Chapter 1, **2010**; b) S. V. Eliseeva, J.-C. G. Bünzli, *Chem. Soc. Rev.* **2010**, *39*, 189 – 227; c) R. Carr, N. H. Evans, D. Parker, *Chem. Soc. Rev.* **2012**, *41*, 7673 – 7686; d) A. D'Aléo, L. Ouahab, C. Andraud, F. Pointillart, M. O. Maury, *Coord. Chem. Rev.* **2012**, *256*, 1604 – 1620.

[2] a) C. P. Montgomery, B. S. Murray, E. J. New, R. Pal, D. Parker, *Acc. Chem. Res.* **2009**, *42*, 925; b) E. G. Moore, A. P. S. Samuel, K. N. Raymond, *Acc. Chem. Res.* **2009**, *42*, 542; c) M. C. Heffern, L. M. Matosziuk and T. J. Meade, *Chem. Rev.* **2014**, *114*, 4496 – 4539.

[3] a) S. Faulkner, S. J. A. Pope, B. P. Burton-Pye, *Appl. Spectro. Rev.* **2005**, *40*, 1; b) E. J. New, D. Parker, D. G. Smith, J. W Walton, *Curr.Opin. Chem. Biol.* **2010**, *14*, 238 – 246.

[4] a) A. Picot, A. D'Aléo, P. L. Baldeck, A. Grichine, A. Duperray, C. Andraud, O. Maury, *J. Am. Chem. Soc.* **2008**, *130*, 1532; b) G.-L. Law, K.-L. Wong, C. W.-Y. Man, W.-T. Wong, S.-W. Tsao, M. H.-W. Lam, P. K.-S. Lam, *J. Am. Chem. Soc.* **2008**, *130*, 3714; c) F. Kielar, A. Congreve, G.-l. Law, E. J. New, D. Parker, K.-L. Wong, P. Castreno, J. de Mendoza, *Chem. Commun.* **2008**, 2435; d) C. Andraud, O. Maury, *Eur. J. Inorg. Chem.* **2009**, *2009*, 4357.

[5] a) S. Pandya, J. Yu, D. Parker, *Dalton Trans.* **2006**, 2757; b) S. Mizukami, K. Tonai, M. Kaneko, K. Kikuchi, *J. Am. Chem. Soc.* **2008**, *130*, 14376 – 14377; c) C. M. G. dos Santos, A. J. Harte, S. J. Quinn, T. Gunnlaugsson, *Coord. Chem. Rev.* **2008**, *252*, 2512 – 2527.

[6] a) F. Degorce, A. Card, S. Soh, E. Trinquet, G. P. Knapik, B. Xie, *Curr. Chem. Genomics* **2009**, *3*, 22 – 32; b) P. Scholler, J. M. Zwier, E. Trinquet, P. Rondard, J.-P. Pin, L. Prézeau, J. Kniazeff, *Prog. Mol. Biol. Transl. Sci.* **2013**, *113*, 275 – 312; c) J. M. Zwier, H. Bazin, L. Lamarque, G. Mathis, *Inorg. Chem.* **2014**, *53*, 1854 – 1866.

[7] a) G. Marriott, R. M. Clegg, D. J. Arnt-Jovin, T. Jovin, *Biophys. J.* **1991**, *60*, 1374 – 1387; b) A. Beeby, S. W. Botchway, I. M. Clarkson, S. Faulkner, A. W. Parker, D. Parker, J. A. G. Williams, *J. Photochem. Photobiol. B* **2000**, *57*, 83 – 89; c) V. Fernández-Moreira, B. Song, V. Sivagnanam, A.-S. Chauvin, C. D. B. Vandevyver, M. A. M. Gijs, I. A. Hemmilä, H.-A. Lehrand, J.-C. G. Bünzli, *Analyst* **2010**, *135*, 42; d) H. E. Rajapakse, N. Gahlaut, S. Mohandessi, D. Yu, J. R. Turner, L. W. Miller, *Proc. Natl. Acad. Sci. USA* **2010**, *107*, 13582 – 13587.

[8] M. Latva, H. Takalo, V.-M. Mukkala, C. Matachescu, J. C. Rodriguez-Ubis, J. Kankare, *J. Lumin.* **1997**, *75*, 149 – 169.

[9] a) B. Alpha, J.-M. Lehn, G. Mathis, *Angew. Chem.* **1987**, *99*, 259; *Angew. Chem. Int. Ed. Engl.* **1987**, *26*, 266; b) S. Petoud, S. M. Cohen, J.-C. G. Bünzli, K. N. Raymond, *J. Am. Chem. Soc.* **2003**, *125*, 13324; c) A. Bourdolle, M. Allali, J.-C. Mulatier, B. Le Guennic, J. M. Zwier, P. L. Baldeck, J.-C. G. Bünzli, C. Andraud, L. Lamarque, O. Maury, *Inorg. Chem.* **2011**, *50*, 4987.

[10] a) E. Deiters, B. Song, A.-S. Chauvin, C. D. B. Vandevyver, F. Gumy, J.-C. G. Bünzli, *Chem. Eur. J.* **2009**, *15*, 885 – 900; b) S. V. Eliseeva, G. Auböck, F. van Mourik, A. Cannizzo, B. Song, E. Deiters, A.-S. Chauvin, M. Chergui, J.-C. G. Bünzli, *J. Phys. Chem. B* **2010**, *114*, 2932.

[11] a) V.-M. Mukkala, C. Sund, M. Kwiatkowski, P. Pasanen, M. Högberg, J. Kankare, H. Takalo, *Helv. Chim. Acta* **1992**, *75*, 1621; b) G. Piszczek, B. P. Maliwal, I. Gryczynski, J. Dattelbaum, J. R. Lakowicz, *J. Fluoresc.* **2001**, *11*, 101 – 107; c) P. Kadjane, M. Starck, F. Camerel, D. Hill, N. Hildebrandt, R. Ziessel, L. J. Charbonnière, *Inorg. Chem.* **2009**, *48*, 4601; d) N. N. Katia, A. Lecointre, M. Regueiro-Figueroa, C. Platas-Iglesias, L. J. Charbonnière, *Inorg. Chem.* **2011**, *50*, 1689; e) M. Starck, P. Kadjane, E. Bois, B. Darbouret, A. Incamps, R. Ziessel, L. J. Charbonnière, *Chem. Eur. J.* **2011**, *17*, 9164 – 9179.

[12] a) M. Li, P. R. Selvin, *J. Am. Chem. Soc.* **1995**, *117*, 8132; b) Y. Bretonnière, M. J. Cann, D. Parker, R. Slater, *Org. Biomol. Chem.* **2004**, *2*, 1624 – 1632.

[13] a) H. Takalo, I. Hemmilä, T. Sutela, M. Latva, *Helv. Chim. Acta* **1996**, *79*, 789; b) C. Gateau, M. Mazzanti, J. Pecaut, F. A. Dunand, L. Helm, *Dalton Trans.* **2003**, 2428; c) G. Nocton, A. Nonat, C. Gateau, M. Mazzanti, *Helv. Chim. Acta* **2009**, *92*, 2257.

[14] a) J. W. Walton, L. Di Bari, D. Parker, G. Pescitelli, H. Puschmann, D. S. Yufit, *Chem. Commun.* **2011**, *47*, 12289; b) J. W. Walton, R. Carr, N. H. Evans, A. M. Funk, A. M. Kenwright, D. Parker, D. S. Yufit, M. Botta, S. De Pinto, K-L. Wong, *Inorg. Chem.* **2012**, *51*, 8042.

[15] A. D'Aléo, A. Bourdolle, S. Bulstein, T. Fauquier, A. Grichine, A. Duperray, P. L. Baldeck, C. Andraud, S. Brasselet, O. Maury, *Angew. Chem. Int. Ed.* **2012**, *51*, 6622 – 6625.

[16] a) J. W. Walton, A. Bourdolle, S. J. Butler, M. Soulie, M. Delbianco, B. K. McMahon, R. Pal, H. Puschmann, J. M. Zwier, L. Lamarque, O. Maury, C. Andraud, D. Parker, *Chem. Commun.* **2013**, *49*, 1600 – 1602; b) L. Lamarque, O. Maury, D. Parker, J. Zwier, J. W. Walton, A. Bourdolle, PCT Int. Appl. (2013), WO 2013011236 A1 20130124; c) V. Placide, D. Pitrat, A. Grichine, A. Duperray, C. Andraud, O. Maury, *Tetrahedron Lett.* **2014**, *55*, 1357 – 1361; d) A. J. Palmer, S. H. Ford, S. J. Butler, T. J. Hawkins, P. J. Hussey, R. Pal, J. W. Walton, D. Parker, *RCS Adv.* **2014**, *4*, 9356 – 9366; e) S. J. Butler, L. Lamarque, R. Pal, D. Parker, *Chem. Sci.* **2014**, *5*, 1750 – 1756.

[17] a) A. Picot, F. Malvolti, B. Le Guennic, P. L. Baldeck, J. A. G. Williams, C. Andraud, O. Maury, *Inorg. Chem.* **2007**, *46*, 2659 – 2665; b) A. D'Aléo, A. Picot, A. Beeby, J. A. G. Williams, B. Le Guennic, C. Andraud, O. Maury, *Inorg. Chem.* **2008**, *47*, 10258 – 10268.

[18] a) S. J. Butler, B. K. McMahon, R. Pal, D. Parker, J. W. Walton, *Chem. Eur. J.* **2013**, *19*, 9511 – 9517; b) B. K. McMahon, R. Pal, D. Parker, *Chem. Commun.* **2013**, *49*, 5363 – 5365.

[19] a) K. Sénéchal-David, A. Hemeryck, N. Tancrez, L. Toupet, J. A. G. Williams, I. Ledoux, J. Zyss, A. Boucekkine, J.-P. Guégan, H. Le Bozec, O. Maury, *J. Am. Chem. Soc.* **2006**, *128*, 12243 – 12255; b) F. Pointillart, B. Le Guennic, O. Maury, S. Golhen, O. Cador, L. Ouahab, *Inorg. Chem.* **2013**, *52*, 1398 – 1408.
[20] M. H. V. Werts, R. T. F. Jukes, J. W. Verhoeven, *Phys. Chem. Chem. Phys.* **2002**, *4*, 1542.
[21] A. Beeby, L. M. Bushby, D. Maffeo, J. A. G. Williams, *J. Chem. Soc. Dalton Trans.* **2002**, 48 – 54.
[22] T. Gallavardin, M. Maurin, S. Marotte, T. Simon, A.-M. Gabudean, Y. Bretonnière, M. Lindgren, F. Lerouge, P. L. Baldeck, O. Stéphan, Y. Leverrier, J. Marvel, S. Parola, O. Maury, C. Andraud, *Photochem. Photobiol. Sci.* **2011**, *10*, 1216 – 1225.
[23] A. Picot, A. D'Aléo, P. L. Baldeck, C. Andraud, O. Maury, *Inorg. Chem.* **2008**, *47*, 10269 – 10279.
[24] Two-photon cell-imaging studies will be reported elsewhere. The resulting images are qualitatively identical under one- and two-photon excitation.
[25] E. J. New, A. Congreve, D. Parker, *Chem. Sci.* **2010**, *1*, 111.
[26] B. Wang, Y. Liang, H. Dong, T. Tan, B. Zhan, J. Cheng, K. K-W. Lo, Y. W. Lam, S. H. Cheng, *ChemBioChem* **2012**, *13*, 2729 – 2737.
[27] a) G.-L. Law, R. Pal, L.-O. Palsson, D. Parker, K-L. Wong, *Chem. Commun.* **2009**, 7321 – 7323; b) J. A. G. Williams, D. Parker, P. K. Senanayake, *J. Chem. Soc. Perkin Trans. 2* **1998**, 2129.
[28] M. J. Frisch, G. W. Trucks, H. B. Schlegel, G. E. Scuseria, M. A. Robb, J. R. Cheeseman, G. Scalmani, V. Barone, B. Mennucci, G. A. Petersson, H. Nakatsuji, M. Caricato, X. Li, H. P. Hratchian, A. F. Izmaylov, J. Bloino, G. Zheng, J. L. Sonnenberg, M. Hada, M. Ehara, K. Toyota, R. Fukuda, J. Hasegawa, M. Ishida, T. Nakajima, Y. Honda, O. Kitao, H. Nakai, T. Vreven, J. A. Montgomery, Jr., J. E. Peralta, F. Ogliaro, M. Bearpark, J. J. Heyd, E. Brothers, K. N. Kudin, V. N. Staroverov, R. Kobayashi, J. Normand, K. Raghavachari, A. Rendell, J. C. Burant, S. S. Iyengar, J. Tomasi, M. Cossi, N. Rega, J. M. Millam, M.; Klene, J. E. Knox, J. B. Cross, V. Bakken, C. Adamo, J. Jaramillo, R. Gomperts, R. E. Stratmann, O. Yazyev, A. J. Austin, R. Cammi, C. Pomelli, J. W. Ochterski, R. L. Martin, K. Morokuma, V. G. Zakrzewski, G. A. Voth, P. Salvador, J. J. Dannenberg, S. Dapprich, A. D. Daniels, O. Farkas, J. B. Foresman, J. V. Ortiz, J. Cioslowski, D. J. Fox Gaussian 09 Revision A.02, Gaussian Inc., Wallingford CT, **2009**.
[29] a) C. Adamo, V. Barone, *J. Chem. Phys.* **1999**, *110*, 6158 – 6170; b) M. Ernzerhof, G. E. Scuseria, *J. Chem. Phys.* **1999**, *110*, 5029.
[30] M. Dolg, H. Stoll, H. Preuss, *Theor. Chem. Acc.* **1993**, *85*, 441.
[31] F. Weigend, R. Ahlrichs, *Phys. Chem. Chem. Phys.* **2005**, *7*, 3297.
[32] C. Xu, W. W. Webb, *J. Opt. Soc. Am. B* **1996**, *13*, 481 – 491.

Received: February 28, 2014
Published online on June 17, 2014